Supporting Information

Au_3Cu Tetrapod Nanocrystals: Highly Efficient and Metabolizable Multimodality Imaging-Guided NIR-II Photothermal Agents

Zhiyi Wang,[a,b,‡] Yanmin Ju,[c,a,‡] Shiyan Tong,[a] Hongchen Zhang,[a] Jian Lin,[d] Baodui Wang,*[,b] Yanglong Hou*[,a]

[a] Beijing Key Laboratory for Magnetoelectric Materials and Devices, Department of Materials Science and Engineering, College of Engineering, Peking University, Beijing Innovation Centre for Engineering Science and Advanced Technology, Beijing 100871, China.

[b] State Key Laboratory of Applied Organic Chemistry and Key Laboratory of Nonferrous Metal Chemistry and Resources Utilization of Gansu Province and, Lanzhou University, Gansu, Lanzhou, 730000, China.

[c] College of Life Science, Peking University, Beijing 100871, China.

[d] Synthetic and Functional Biomolecules Center, Department of Chemical Biology, College of Chemistry and Molecular Engineering, Peking University, Beijing 100871, China.

‡ These authors contributed equally.

Supplementary Methods:

Materials. All the chemicals were used without further purification. Hydrogen tetrachloroaurate (III) hydrate ($HAuCl_4•3H_2O$, 99.8%) were purchased from STREM. Tri-n-octlamine (TOA, 97%), 1-Octadecene (ODE, tech. 90%) and 1-Hexadecylamine (90%) were purchased from Alfa Asear. Copper (II) chloride dehydrate ($CuCl_2•2H2O$, 99.9%), Ammonium chloride (NH_4Cl, 99%), D-(+)-Glucose (98%), 1,2,3,4-Tetrahydronaphthalene (97%) and borane-tert-butylamine complex (TBAB, 97%) were purchased from J&K Chemicals. Copper (II) acetylacetonate ($Cu(acac)_2$, 99%), Oleylamine (OAm, 70 %), Oleic acid (OAc, 90%), N,N'-dicyclohexylcarbodiimide (DCC, 99%), calcein-AM and propidium iodide (PI) were purchased from Sigma Aldrich. Deionized water (18.2 MΩ•cm resistivity at room temperature) was used for all tests. HS-PEG-NH_2, HS-PEG-Cy5 and HS-PEG-FA were prepared according to the literature.[1]

Measurements. X-ray photoelectron spectroscopy (XPS) measurements were performed on an Imaging X-ray Photoelectron Spectrometer using Al Kα radiation (Axis Ultra, SHIMADZU, Japan).

The emission spectra were recorded on a Shimadzu RF-5301 spectrophotometer. X-ray diffraction (XRD) patterns were carried out using a Rigaku DMAX-2400 X-ray diffractometer equipped with Cu Kα (λ = 0.15405 nm) radiation. Transmission electron microscopy (TEM) images were obtained from an FEI Tecnai T20 microscope. High-resolution TEM (HRTEM) images were obtained from an FEI Tecnai F30 microscope. Reinforced carbon membrane support grid was used to obtain the EDS-mapping. Fluorescence microscopic images were viewed under a fluorescent microscope (Leica DR) equipped with a digital camera (ORCA-ER, Hamamatsu). Photos were processed by using Photoshop software (Adobe, CA). The concentrations of Au and Cu were quantified using an inductively coupled plasma-atomic emission spectrometer (ICP-AES, Prodigy 7, and Leeman, USA). Dynamic light scattering (DLS) was measured using a particle size analyzer (Zetasizer Nano ZS-90, Malvern, England). UV-Vis-NIR absorption spectra were measured on UV-VIS-NIR SPECTROPHOTOMETER (UV3600PLUS, SHIMADZU, and Japan). FT-IR spectra were obtained on Spectrum Spotlight 200 FT-IR microscopy (Spotlight200, PE, and USA). The temperature detection and thermal image record were conducted on an infrared thermal imaging instrument (FLIR A325SC camera). The NIR-I laser was produced using an 808 nm high-power multimode pump laser (Shanghai Connect iber Optics Co.). The NIR-II laser was produced using a 1064 nm high-power multimode pump laser (Shanghai Connect Fiber Optics Co.).

Synthesis of Au seeds. Typically, $HAuCl_4 \cdot 3H_2O$ (0.25 mmol, 103.0 mg), 1,2,3,4-Tetrahydronaphthalene (10 mL) and OAm (10 mL) were mixed in a 100 mL four-necked flask under a high purity nitrogen (99.99%) atmosphere. The system was keep to 25 °C and stirred for 10 min. Then a homogeneous mixture of TBAB (1 mmol, 87.0 mg), 1,2,3,4-tetrahydronaphthalene (1 mL) and OAm (1 mL) was added in this system rapidly and allowed to react for 60 min under the same conditions. After 60 min, Au seeds were washed 3 times with ethyl alcohol and re-dispersed in hexane.

Synthesis of Au_3Cu TPNCs. 1-Hexadecylamine (2 mmol, 536.6 mg), NH_4Cl (0.25mmol, 13.4 mg), Au seeds (10 mg) and deionized water (20 mL) were mixed by magnetic stirring in a 100 mL four-neck flask and degassed under a high purity nitrogen (99.99%) atmosphere at 100 °C for 2 h. Subsequently, the mixed solution containing $HAuCl_4 \cdot 3H_2O$ (0.20 mmol, 41.1 mg), $CuCl_2 \cdot 2H_2O$ (0.10 mmol, 17.0 mg) and D-(+)-Glucose (1 mmol, 180.16 mg) dissolved in 2 mL deionized water was injected to the above system rapidly. The mixed solution was allowed to react for another 40 minutes under the same conditions. After 40 minutes, the Au_3Cu TPNCs were washed for 3 times with ethyl alcohol and re-dispersed in hexane. NH_4F, NH_4Br and NH_4I were also used to control the grow process of the nanocrystals under the same reaction conditions.

Modification of Au_3Cu TPNCs. The modification was carried out according to the literature.[2] Briefly, 2 mL of chloroform containing 5 mg of NCs was added dropwise into 40 mg of HS-PEG-NH_2 which was dissolved in 20 mL of chloroform. The mixed solution was stirred for 12 h under a high purity nitrogen (99.99%) atmosphere. The obtained product was collected by centrifugation and dialyzed with H_2O for 24 h to remove the free ligand. The modification with HS-PEG-Cy5 and HS-PEG-FA was similar with HS-PEG-NH_2. The obtained products were denoted as Au_3Cu@PEG TPNCs, Au_3Cu@PEG-FA, Au_3Cu@PEG-Cy5 and Au_3Cu@PEG-Cy5,FA, respectively.

Photothermal effect, photostability, and photothermal conversion efficiency. A series of Au_3Cu@PEG TPNCs solutions with concentrations of 0, 10, 20, 40, 60 and 80 μg L^{-1} were irradiated with an 808 nm laser (1.0 W cm^{-2}) and 1064 nm (0.8 W cm^{-2}) laser for 15 min (Hi-Tech Optoelectronics Co., Ltd. Beijing, China), and their temperature in solution was recorded by an online type thermocouple thermometer (DT-8891E Shenzhen Everbest Machinery Industry Co., Ltd., China) with an accuracy of ±0.1 °C. Similarly, in order to study the influence of optical density on photothermal conversion, 400 μL of 40 μg L^{-1} Au_3Cu@PEG TPNCs solution was irradiated with an 808 nm laser and 1064 nm laser with different power density for 5 min. The change of temperature in solution was recorded by an online type thermocouple thermometer with an accuracy of ±0.1 °C. The photostability of Au_3Cu@PEG TPNCs was estimated by irradiating 40 μg L^{-1} solution in a quartz cuvette with an 808 (1.0 W cm^{-2}) and 1064 nm laser (0.8 W cm^{-2}) for 5 min (laser on) and then cooling to room temperature without irradiation (laser off). Such heating/cooling processes were repeated four times to test the photostability. To determine the photothermal conversion efficiency (η) of Au_3Cu@PEG TPNCs, 40 μg L^{-1} solution was continuously irradiated with an 808 (1.0 W cm^{-2}) or 1064 nm laser (0.8 W cm^{-2}) to reach a steady temperature, and then the laser was turned off to allow the solution to naturally cool down to room temperature. The calculation details are given in the Supporting Information.

Deep-tissue photothermal therapy in NIR-I and NIR-II windows. The NIR-II window can supply higher tissue penetration depth than the commonly used exploration NIR-I window, due to its lower absorption and scattering by tissues in this spectral range. We evaluated the residual laser-energy density of chicken breast muscles with different thickness (0, 2, 4, 6, 8, and 10 mm) after penetration under 808 and 1064 nm laser irradiation. Then, we further explored the deep tissue photothermal capability in NIR-I and NIR-II windows using the synthesized the tetrapod-shaped Au_3Cu TPNCs with above chicken breast muscles under the laser irradiations. 5 mL tubes filled with 200 μL portion of tetrapod-shaped Au_3Cu TPNCs dispersion covered with the tissues of different thicknesses were

subjected to 808 and 1064 nm laser irradiation (0.8 W cm^{-2}) for 5 min, and the infrared thermographs were then captured by a thermal imaging camera.

***In vitro* photothermal ablation of cancer cells.** NIH3T3 and KB cells (1×10^4 cells per well) seeded into a 96-well cell culture plate were incubated with Au_3Cu@PEG TPNCs in different concentrations (0, 0.625, 1.25, 2.50, 5.00, 10.0, 20.0 and 40.0 μg L^{-1}) for 24 h at 37 °C under 5% CO_2. The cells were washed three times with PBS and fed with fresh medium, followed by irradiating for 5 min under the irradiation of an 808 and 1064 nm (λ) laser with a power density of 1.0 W cm^{-2} and 0.8 W cm^{-2} respectively. Finally, a standard CCK-8 assay was used to evaluate the viability of cells (n = 3).

To examine the photothermal effect of Au_3Cu@PEG TPNCs on KB cells *in vitro*, KB cells seeded (1×10^4 cells per well) in culture dishes were incubated with Au_3Cu@PEG TPNCs (40 μg L^{-1}, 100 μL) for 4 h, when cells of each disk reached 80% confluence. The adherent cell solution was irradiated by an 808 and 1064 nm laser for 5 min under a power density of 1.0 W cm^{-2} and 0.8 W cm^{-2} respectively. After the DMEM medium was removed, the cells washed with PBS over three times. KB cells were incubated with calcein-AM (100 μL) and PI solution (100 μL) for 15 min. Living cells and dead cells were stained with calcein-AM (green fluorescence) and PI (red fluorescence) solution, respectively.

***In vitro* and *in vivo* fluorescence imaging.** For *in vitro* fluorescence imaging, NIH3T3 cells and KB cells seeded in 6-well plates were incubated with Au_3Cu@PEG-Cy5,FA (100 μL, 40 μg L^{-1}) for 15min at 37 ^{0}C under 5% CO_2. After washing the cells three times with PBS buffer the fluorescence images was performed by a Zeiss Leica inverted epifluorescence/reflectance laser scanning confocal microscope. The excitation was at 646 ± 5 nm, and the emission was at 668 ± 5 nm.

For fluorescence imaging *in vivo*, the KB-tumor-bearing mice were intravenously administered with Au_3Cu@PEG-Cy5,FA samples (20 mg/kg, 200 μL). After the injection, the fluorescence signal was recorded on the CRi maestro ex *in vivo* imaging system (USA) at different time points (0, 3, 6, 12, 24, and 48 h). The fluorescence signal before injection was used as the control. To confirm the *in vivo* distribution of Au_3Cu@PEG-Cy5,FA, mice were sacrificed 10 h post-injection. The liver, heart, lung, spleen, tumor, and kidneys were collected for imaging and semi quantitative biodistribution analysis.

***In vivo* photoacoustic tomography.** Mice with tumor volumes (at the right back) of 100-200 mm^3 were used for *in vivo* photoacoustic imaging by multispectral optical tomography system (MSOT inVision 128, iThera medical, Germany). Mice were randomly allocated into two groups, 200μL 20

mg/kg Au_3Cu@PEG-Cy5,FA or Au_3Cu@PEG-Cy5 were administered *via* tail vein respectively. Photoacoustic signals were detected under wavelength of 1064 nm. The oxygenated and deoxygenated hemoglobin were measured at two excitation wavelengths of two 850 nm and 1064 nm, respectively. MSOT signals before injection were recorded as a control.

Calculation of the extinction coefficient. We first measured the absorbance of Au_3Cu@PEG TPNCs with different concentrations of 6.6, 13.2, 19.8, 26.4 and 33.0 μg L^{-1} at 808 and1064 nm. The extinction coefficient ε (λ) of the Au_3Cu TPNCs is determined according to the Lambert-Beer law A(λ) = εLC (where A is the absorbance at a wavelength of λ, L is the pathlength (1cm), and C is the concentration of the NCs). The extinction coefficient ε is calculated by plotting the slope (in $Lg^{-1}cm^{-1}$) of each linear fit against wavelength. The 808 and 1064 nm laser extinction coefficient (ε) of Au_3Cu TPNCs can be measured to be 33.1 and 53.0 $Lg^{-1}cm^{-1}$, respectively.

In vitro cytotoxicity assay. NIH3T3 or KB cells (1×10^4 cells per well) seeded into a 96-well cell culture plate were incubated with Au_3Cu@PEG TPNCs in different concentrations (0, 0.625, 1.25, 2.50, 5.00, 10.0, 20.0 and 40.0 μg mL^{-1}) for 24 h at 37 °C under 5% CO_2. The relative cell viabilities were determined by a standard CCK-8 viability assay (Cell Counting Kit, Dojindo Laboratories, Kumamoto, Japan).

Hemolysis Assay. Human blood was obtained from from a healthy human donor. Briefly, 5% suspension of RBCs (0.2 mL) was used for this purpose after three washings along with 0.8 mL different concentrations (0, 0.625, 1.25, 2.50, 5.00, 10.0, 20.0 and 40.0 μg mL^{-1}) of Au_3Cu TPNCs and Au_3Cu@PEG respectively. Incubation of deionized water and DPBS with RBCs were used as positive control and negative control, respectively. All the samples were kept at room temperature for 3 h. Finally, the mixtures were centrifuged at 1000 rpm for 3 min. The absorbance values of supernatants at 570 nm were determined by using a microplate reader with absorbance at 655 nm as a reference. The hemolysis percentage of RBCs was calculated based on the formula shown below:

$$Hemolysis\ percentage\ (\%) = \frac{sample\ absorbance - negative\ control\ absorbance}{positive\ control\ absorbance\ -\ negative\ control\ absorbance} \times 100$$

In vivo **temperature measurement during NIR irradiation and photothermal therapy.** Solutions of 200 μL 20 mg/kg Au_3Cu@PEG-Cy5,FA, Au_3Cu@PEG-Cy5 and a saline solution were administered by i.v. injection to the KB tumor bearing mice, respectively. Control mice were injected with 200 μL PBS. The mice received NIR irradiation (1064 nm, 0.8 W cm^{-2}) for 5 minutes at 24 h after intravenous injection. The thermographic map of the tumor tissues before and after illumination was imaged by thermal imaging camera (FLIR SC7100, USA). Photothermal ablation was performed

when the tumors reached to about 100-200 mm^3. We divided into 5 groups with 3 mice in each group: (1) Au_3Cu@PEG-Cy5,FA with laser; (2) Au_3Cu@PEG-Cy5 with laser; (3) Au_3Cu@PEG-Cy5,FA only; (4) laser only; (5) control (saline). 1064 nm laser irradiation was carried out 24 h after injection at a power 0.8 W cm^{-2} for 5 min. Tumor sizes and body weights were measured every 3 days during the treatment. Tumor volume was calculated according to the formula of $(a \times b^2)/2$, where a and b are the long and short diameters of the tumor, respectively.

Measurement of Photothermal Performance. There are two main parameters that determine the photothermal performance of nanomaterials, including the extinction coefficient (ε) and photothermal-conversion efficiency (η).[3] The corresponding calculation process was as follows:

(1) Calculation of the Extinction Coefficient. the extinction coefficient $\varepsilon(\lambda)$ of Au_3Cu@PEG TPNCs was determined according to the Lambert−Beer law:

$$A_\lambda = \varepsilon b C \qquad (1)$$

where A is the absorbance at a wavelength of λ, b is the pathlength (1 cm), and C is the concentration of the Au_3Cu@PEG TPNCs. The extinction coefficient ε can be obtained from the slope of the linear region of the absorbance–concentration curve. As a result, the 808 and 1064 nm laser extinction coefficient (ε) of Au_3Cu@PEG TPNCs can be measured to be 33.1 and 53.0 L g^{-1} cm^{-1}, respectively.

(2) Calculation of the Photothermal Conversion Efficiency. The photothermal conversion efficiency (η) is calcuted by the following equations[4-7]:

$$\sum m_i C_{p,i} \frac{dT}{dt} = Q_{in,NCs} + Q_{in,sys} + Q_{out} \quad (Q_{in,NCs} > 0, Q_{in,system} > 0, Q_{out} < 0) \qquad (2)$$

where C_p and m are the heat capacity and the mass of solvent (water), T is the solution temperature, $Q_{in,NCs}$ is the energy input of Au_3Cu TPNCs, $Q_{in,sys}$ is the baseline energy input of the sample cell, and Q_{out} is the heat conducted away from the system surface by air. The NIR laser-induced source term, $Q_{in,NCs}$, expresses heat dissipated by electron−phonon relaxation of the plasmon on the Au_3Cu TPNCs surface under the irradiation of an 808 or 1064 nm (λ) laser:

$$Q_{in,NCs} = I(1-10^{-A_\lambda})\eta \qquad (3)$$

where I is the incident energy of the NIR laser (mW), A_λ is the absorbance of the Au_3Cu TPNCs at the NIR laser wavelength (λ) of 808 or 1064 nm, and η is the photothermal-conversion efficiency from the incident NIR laser energy to thermal energy. Besides, Q_{Dis} represents the heat dissipated from the photoabsorption of the 96-wells plate itself, and it was measured independently to be Q_{Dis}=

69.31 mW (in units of mW) using a sample cell containing pure water without Au_3Cu TPNCs.[1] Q_{surr} is temperature-dependent parameter, which is linear with the output of thermal energy.

$$Q_{out} = hS(T\text{-}T_{surr}) \quad (4)$$

where h represents heat-transfer coefficient, S represents the surface area of the container, T represents the temperature of system surface, and TSurr represents the surrounding temperature. Once the NIR laser power is defined, the heat input ($Q_{in,NCs}$+$Q_{in,sys}$) will be finite. Since the heat output (T_{Surr}) is increased along with the rise in temperature according to eq 5, the temperature of system will reach a maximum when the heat output is equal to heat input

$$Q_{in,NCs} + Q_{in,sys} = -Q_{out} = hS(T_{\max}\text{-}T_{surr}) \quad (5)$$

$$hS = \frac{\sum m_i C_{p,i}}{\tau_S} \quad (6)$$

$$\theta = \frac{T\text{-}T_{surr}}{T_{\max}\text{-}T_{surr}} \quad (7)$$

$$t = -\tau_S ln \frac{T\text{-}T_{surr}}{T_{\max}\text{-}T_{surr}} \quad (8)$$

$$t = -\tau_S ln\theta \quad (9)$$

$$\eta = \frac{hS(T_{\max,H_2O}\text{-}T_{surr})\text{-}Q_{Dis}}{I(1-10^{-A_\lambda})} \quad (10)$$

The result of that case irradiated under 808nm laser is that τ_s = 137.68 s, obtained by linear fitting using linear cooling time (after irradiation and the period is between 300 s and 600 s) and negative natural logarithm of temperature (Figure 4K) after the colloid temperature increased to the final plateau value. The value of m and Cp are 0.400 g and 4.2 J/(g·℃). Therefore, hS is calculated to be 12.20 mW/℃ by using equation (4). Q_{dis} and A_{808nm} are measured independently as 82.71 mW with power (I) 1.0 W and 0.578, respectively.[7] Substituting all of value to parameters into the equation (9), the photothermal conversion efficiency, η, of Au_3Cu TPNCs can be calculated to be 39.45%.

The result of that case irradiated under 1064 nm laser is that τs = 135.62 s, obtained by linear fitting using linear cooling time (after irradiation and the period is between 300 s and 600 s) and negative natural logarithm of temperature (Figure 4L). The value of m and C_p are 0.400 g and 4.2 J/(g·℃). Therefore, hS is calculated as 12.39 mW/℃ by using equation (4). Q_{dis} and A_{1064nm} are measured independently to be 69.31 mW with power density (I) 0.8 W and 0.891 respectively.[7] Substituting all of value to parameters into the equation (9), the photothermal conversion efficiency, η, of Au_3Cu TPNCs can be calculated to be 75.27%.

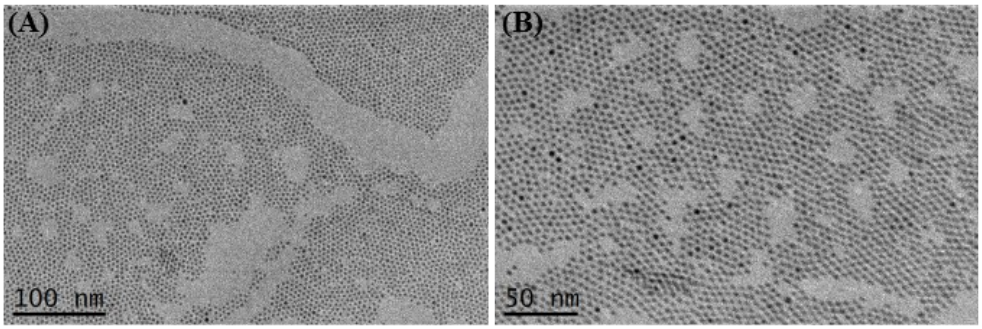

Figure S1. TEM image of Au seeds.

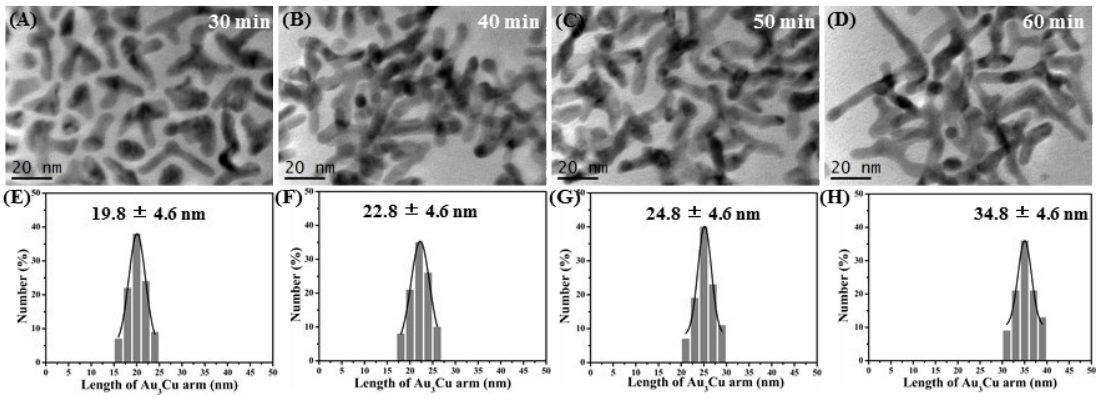

Figure S2. TEM image of Au_3Cu TPNCs and length of Au_3Cu arm at different reaction time: (A-E) 30 min, (B-F) 40 min, (C-G) 50 min, and (D-H) 60 min.

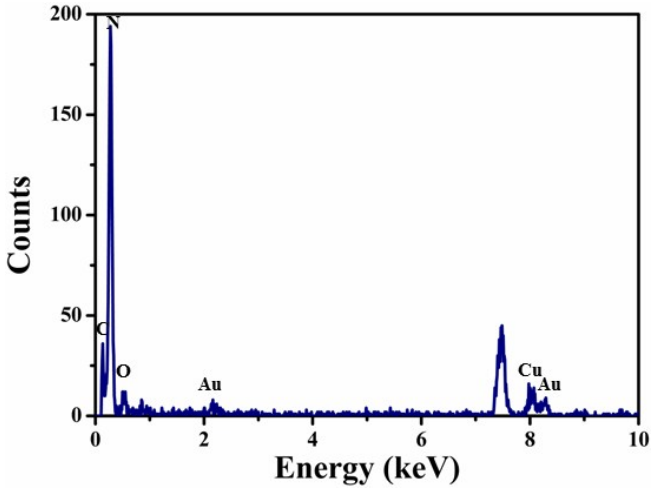

Figure S3. EDX of Au_3Cu TPNCs.

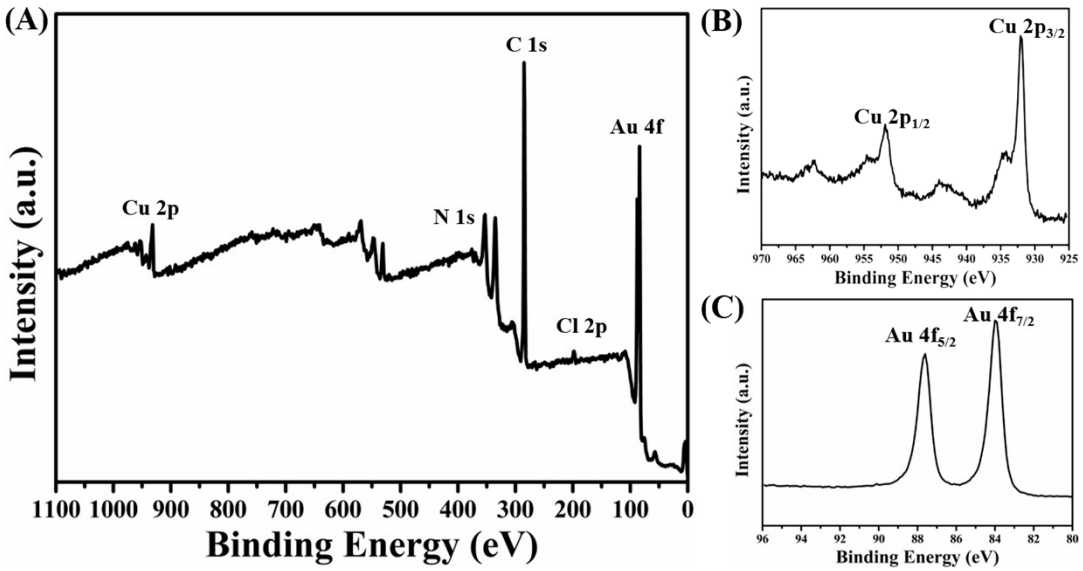

Figure S4. XPS of Au_3Cu TPNCs (A) and High resolution XPS of Cu 2p (B) and Au 4f (C).

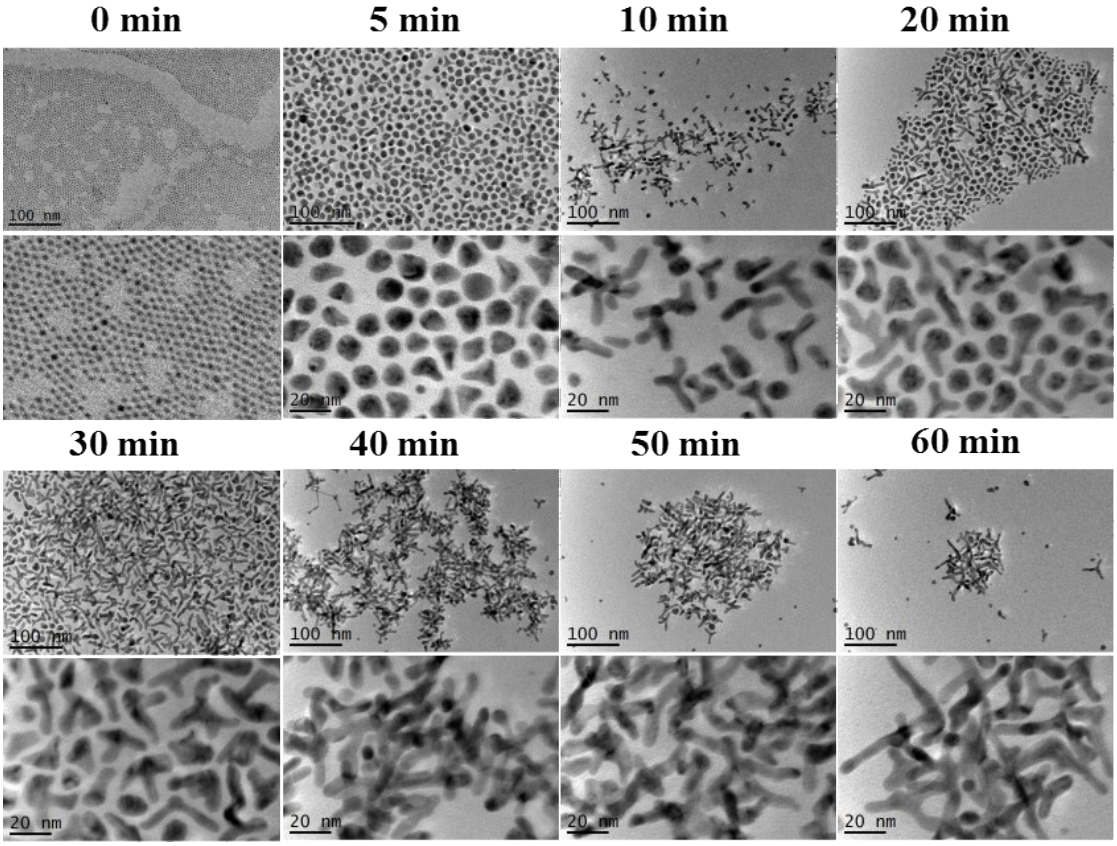

Figure S5. TEM images of the Au_3Cu TPNCs obtained using the standard procedure at different reaction times, showing the evolution of morphology with time.

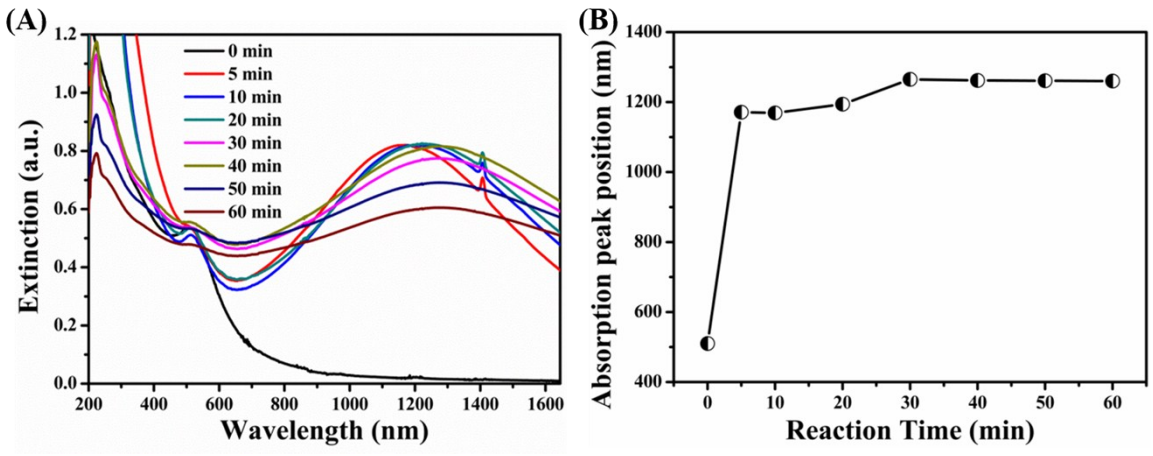

Figure S6. (A) UV-Vis-NIR extinction spectra and (B) Absorption peak position of the obtained NCs in different reaction time.

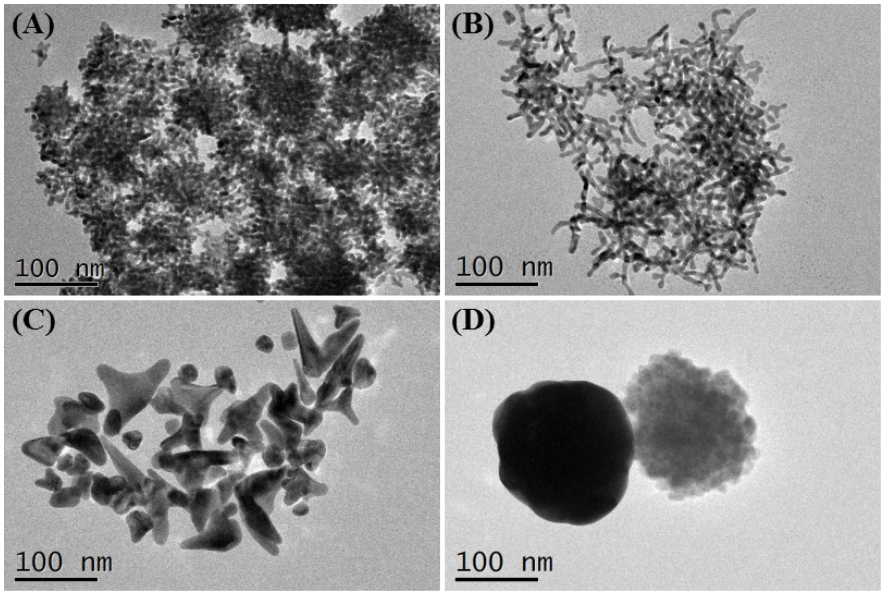

Figure S7. TEM image of the NCs under different reaction condition: (A) no NH_4Cl, (B) NH_4F, (C) NH_4Br and (D) NH_4I.

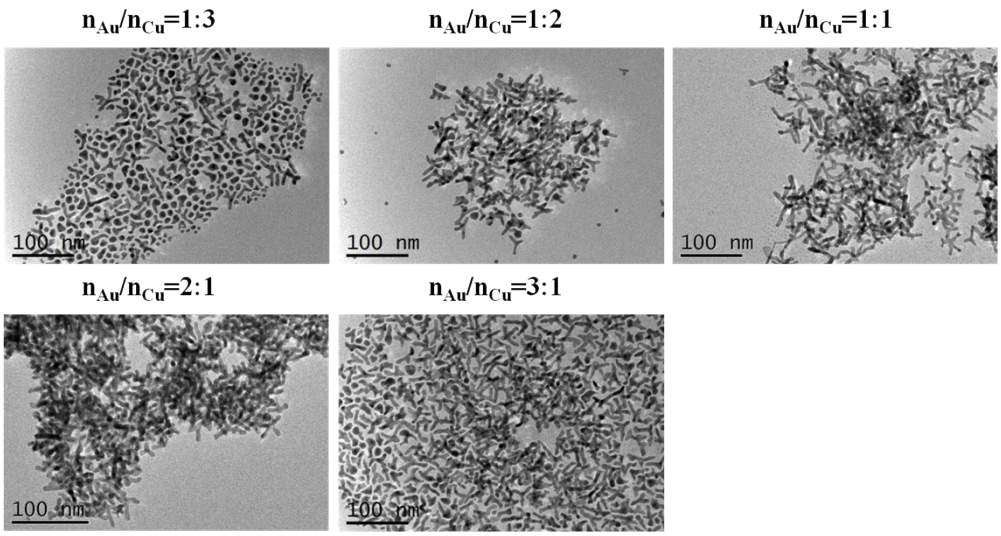

Figure S8. TEM image of the obtained NCs with different n_{Au}/n_{Cu} ratio.

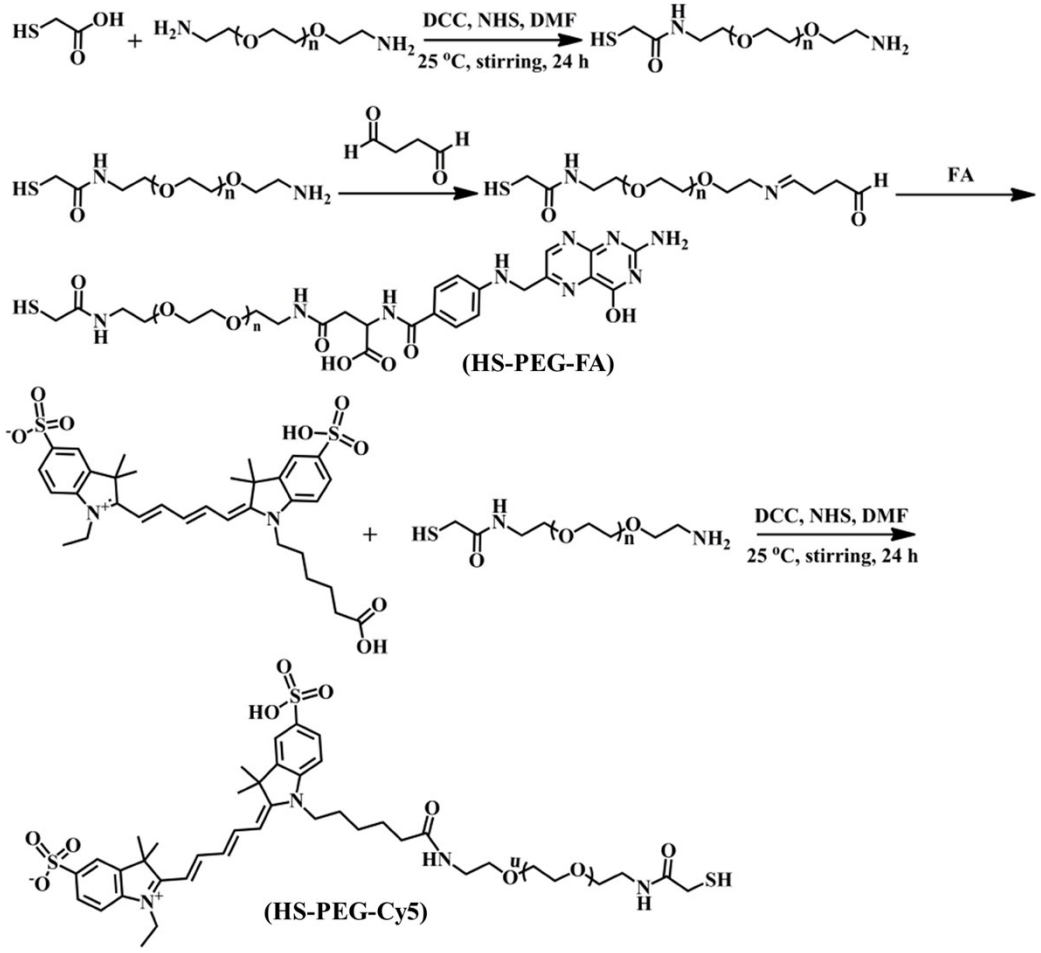

Figure S9. Synthetic route of the molecule for fuctional modification.

Figure S10. The camera picture of Au_3Cu TPNCs, Au_3Cu@PEG, Au_3Cu@PEG-FA, Au_3Cu@PEG-Cy5 and Au_3Cu@PEG-Cy5,FA.

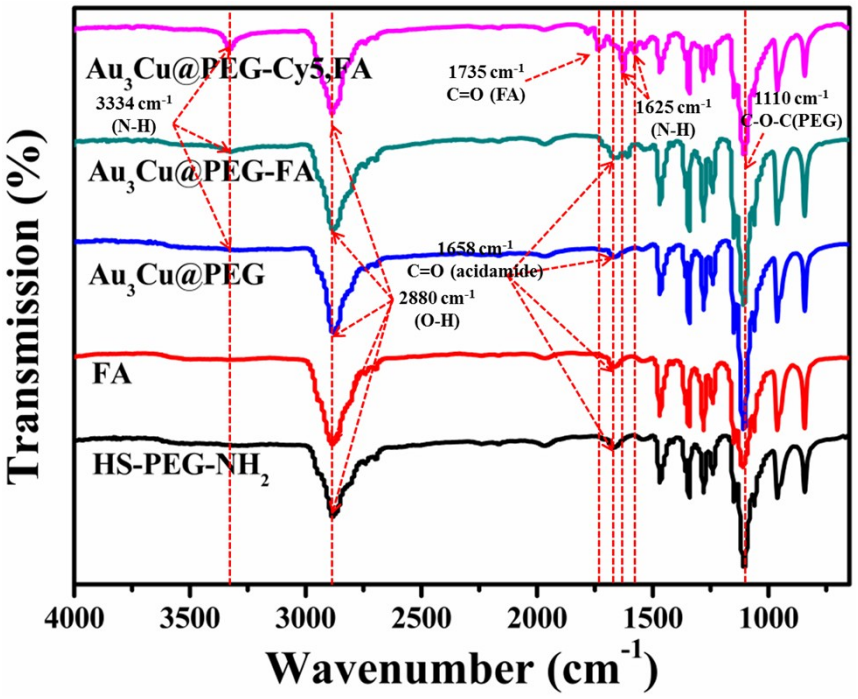

Figure S11. FT-IR characterization of HS-PEG-NH_2 (black line), FA (red line), Au_3Cu@PEG (blue line), Au_3Cu@PEG-FA (green line) and Au_3Cu@PEG-Cy5,FA (purple line).

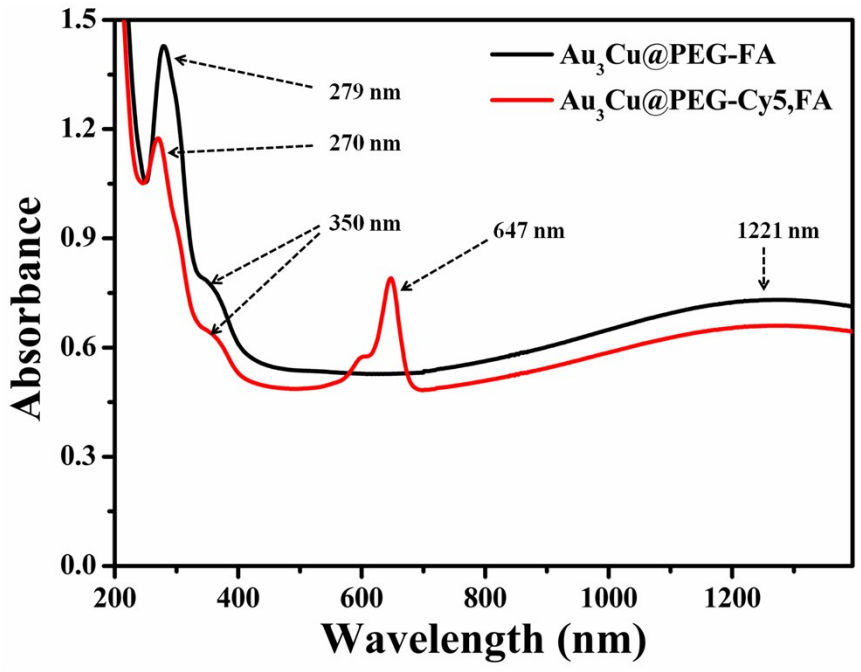

Figure S12. UV-vis absorbance spectra of Au_3Cu@PEG-FA (black line) and Au_3Cu@PEG-Cy5,FA (red line). The absorbance peaks at 270 nm, 279 nm and 350 nm belong to FA. The absorbance peak at 647 nm belongs to Cy5. The absorbance peak at 1221 nm belongs to Au_3Cu TPNCs.

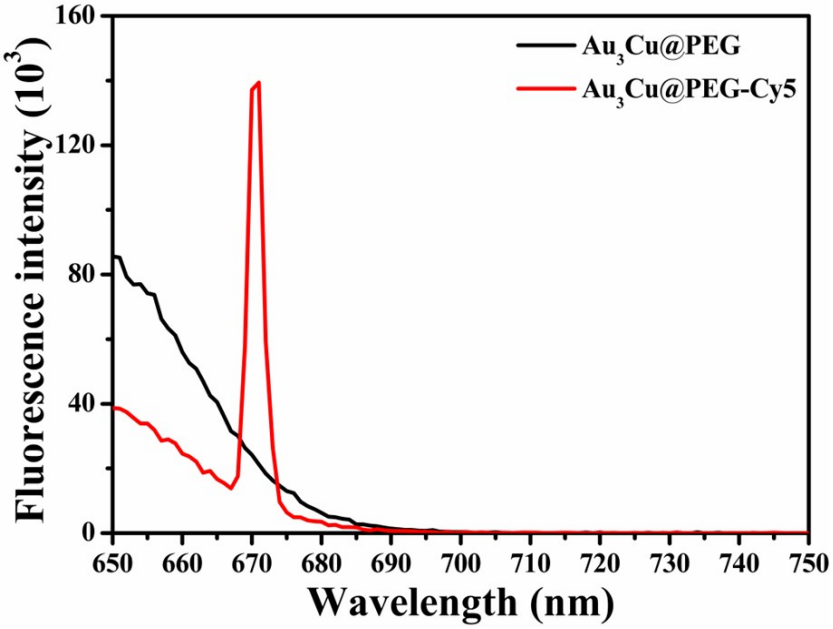

Figure S13. Fluorescence spectrum of Au_3Cu@PEG (black line) and Au_3Cu@PEG-Cy5 (red line). Ex = 645 nm, Em = 669 nm, belonging to Cy5.

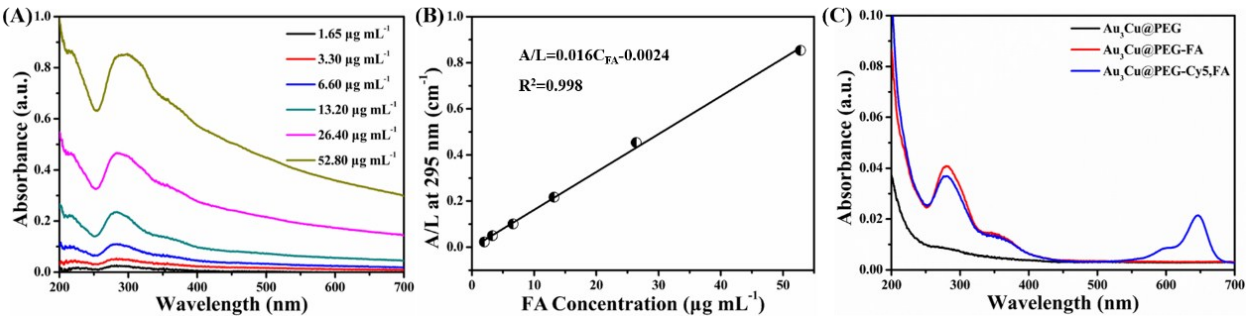

Figure S14. UV-Vis absorption spectra of FA with different concentration (1.65, 3.30, 6.60, 13.20, 26.40 and 52.80 μg mL^{-1}); (B) The linear relationship between FA concentration and A/L (A: the absorbance at 270 nm, L: the width of quartz cell); (C) UV-Vis absorption spectra of Au_3Cu@PEG, Au_3Cu@PEG-FA and Au_3Cu@PEG-Cy5,FA with the same concentration of Au_3Cu TPNCs (3 μg mL^{-1}). FA concentration was determined based on Lambert-Beer law. The quantification of FA in Au_3Cu@PEG-FA and Au_3Cu@PEG-Cy5,FA was calculated by the Linear fitting equation. The results showed 2.18 μg mL^{-1} of FA in Au_3Cu@PEG-FA dispersion and 1.93 μg mL^{-1} of FA in Au_3Cu@PEG- Cy5,FA.

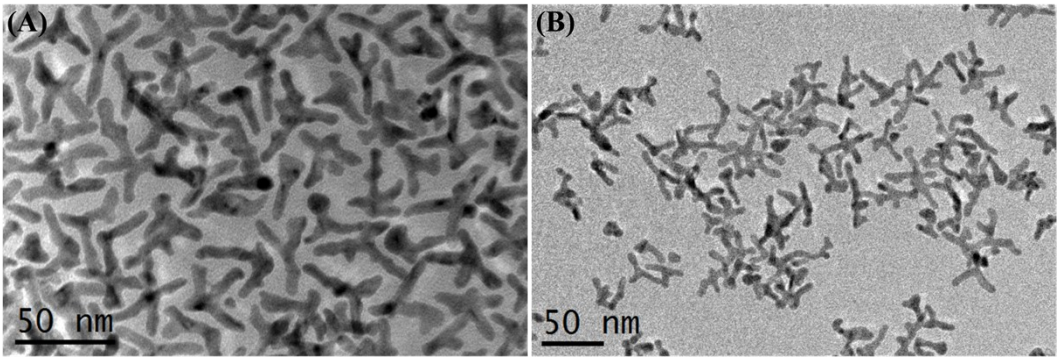

Figure S15. TEM images of Au_3Cu TPNCs in hexane (A) and Au_3Cu@PEG in H_2O (B).

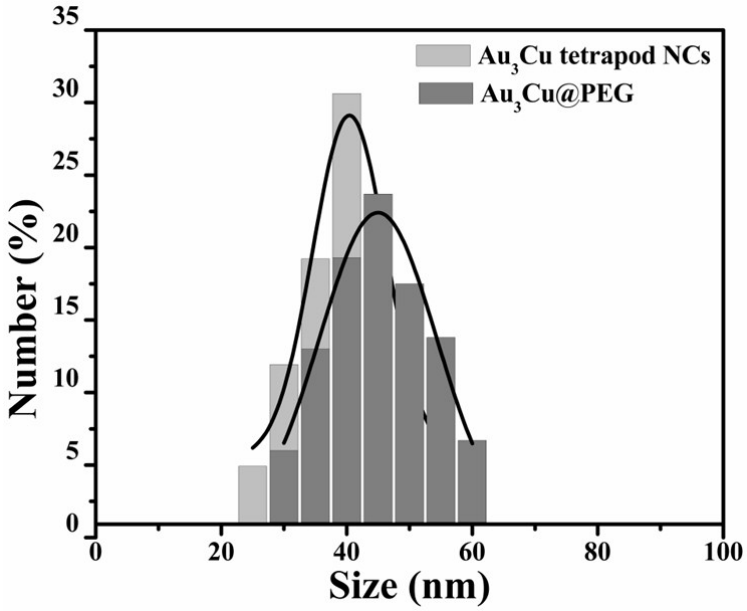

Figure S16. Hydrodynamic diameters measured by DLS for the as-synthesized Au_3Cu TPNCs dispersed in hexane (39.87 nm) and the Au_3Cu@PEG dispersed in PBS (44.93 nm).

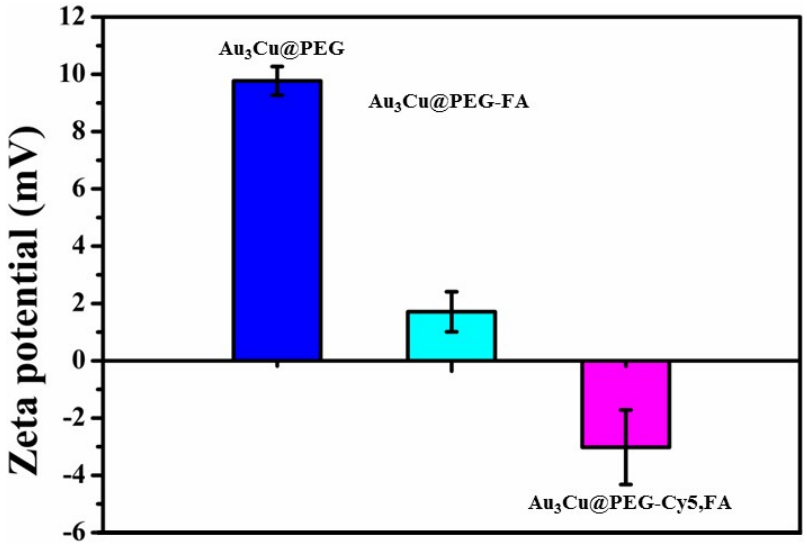

Figure S17. Zeta potential of Au_3Cu@PEG (dark blue), Au_3Cu@PEG-FA (light blue) and Au_3Cu@PEG-Cy5,FA (purple) in deionized water.

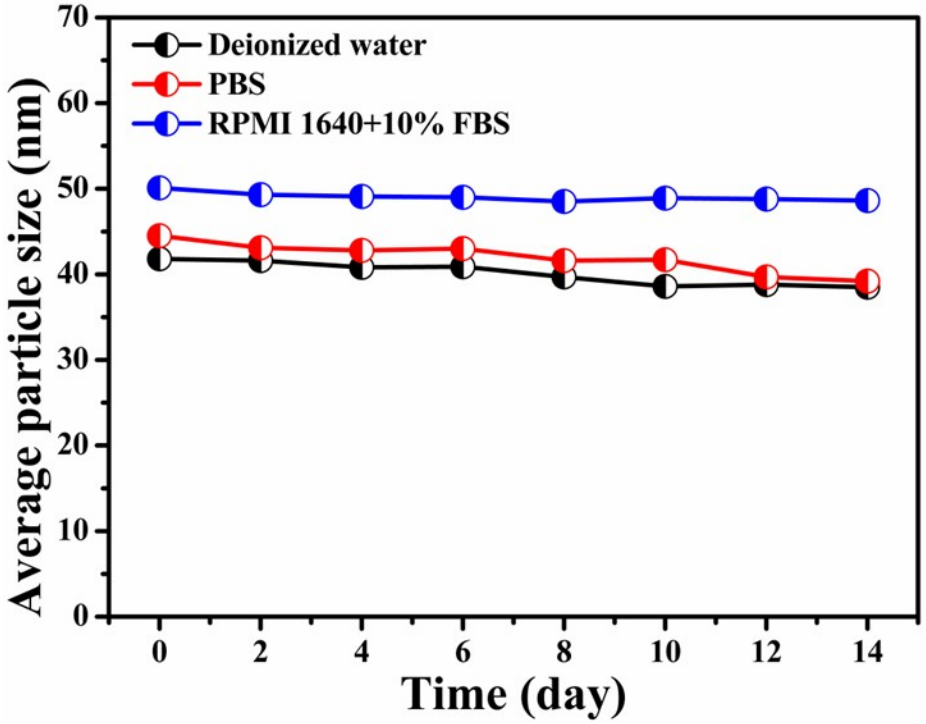

Figure S18. The hydrodynamic diameters of the Au3Cu@PEG dispersed in deionized water, PBS and RPMI 1640+10% FBS for 14 days.

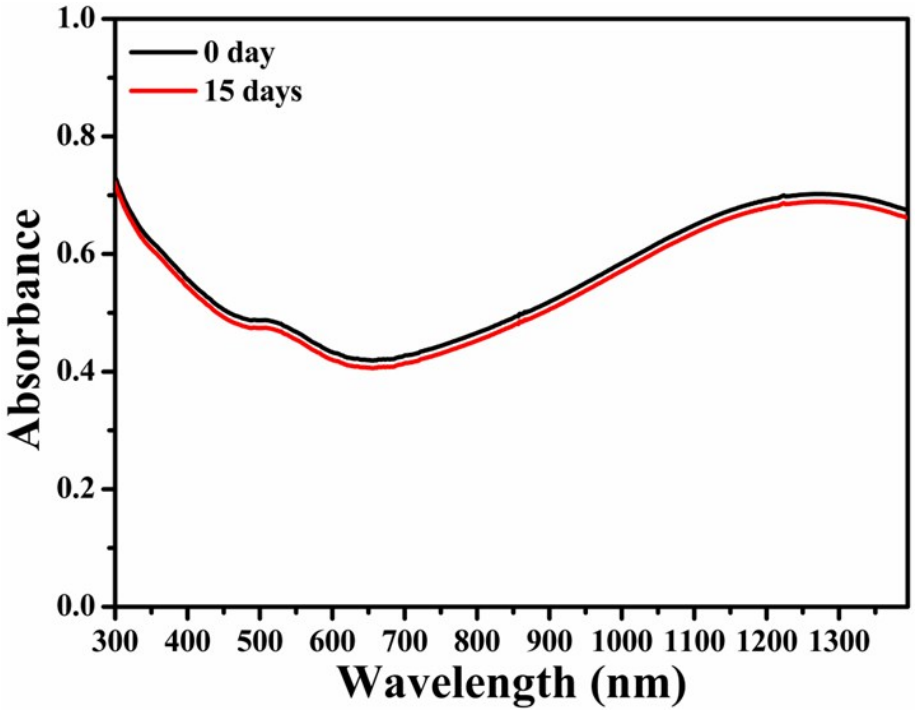

Figure S19. UV-vis detection of Au_3Cu@PEG in PBS solution before (black line) and after 15 days (red line).

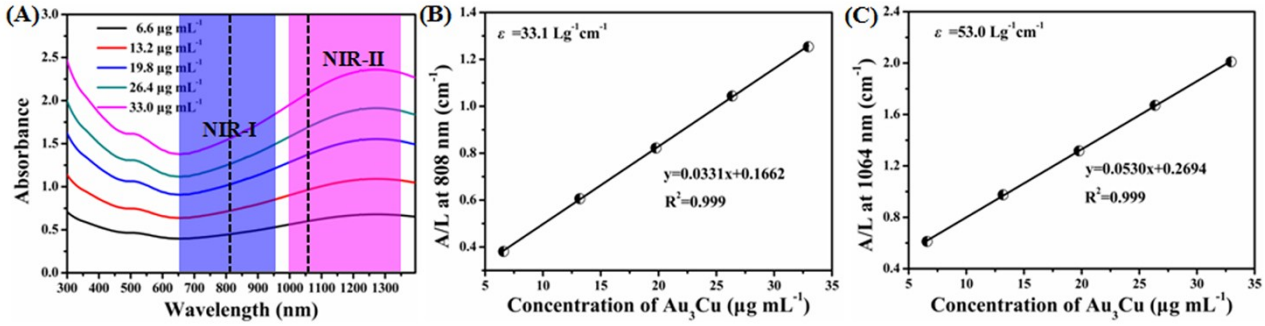

Figure S20. (A) UV-Vis-NIR absorbance spectra of Au_3Cu@PEG TPNCs dispersions at various concentrations (6.6, 13.2, 19.8, 26.4 and 33.0 μg mL^{-1}). Inset: NIR-I (750−950 nm) and NIR-II (1000−1350 nm). Mass extinction coefficient of Au_3Cu@PEG TPNCs at (B) 808 nm and (C) 1064 nm.

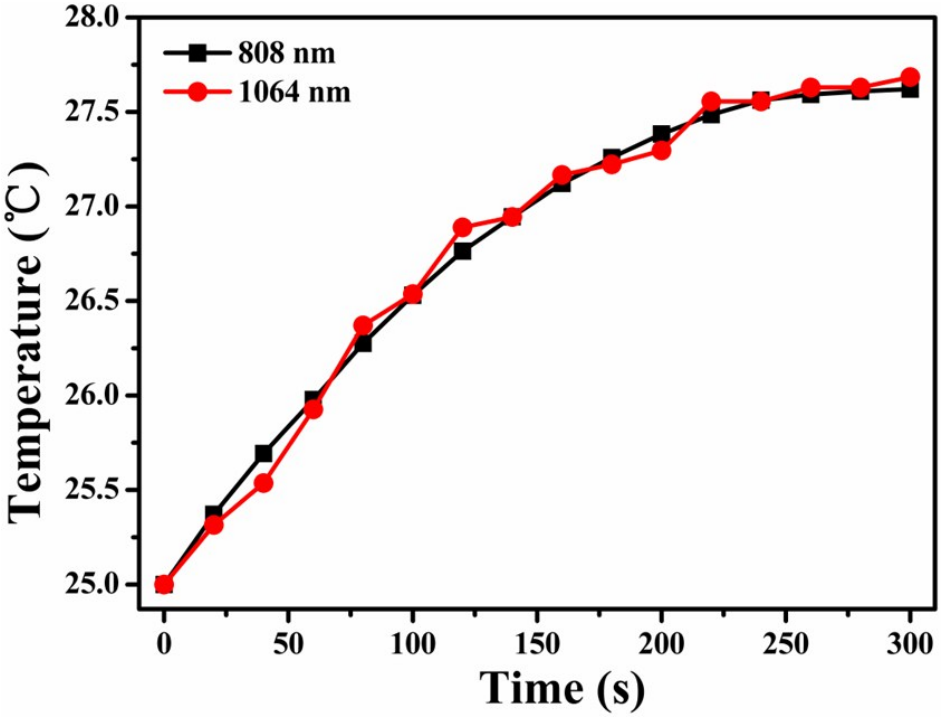

Figure S21. Photothermal heating curves of deionized water at 808 nm (black line) and 1064 nm (red line) laser under 1.0 W cm^{-2} and 0.8 W cm^{-2} laser irradiation respectively.

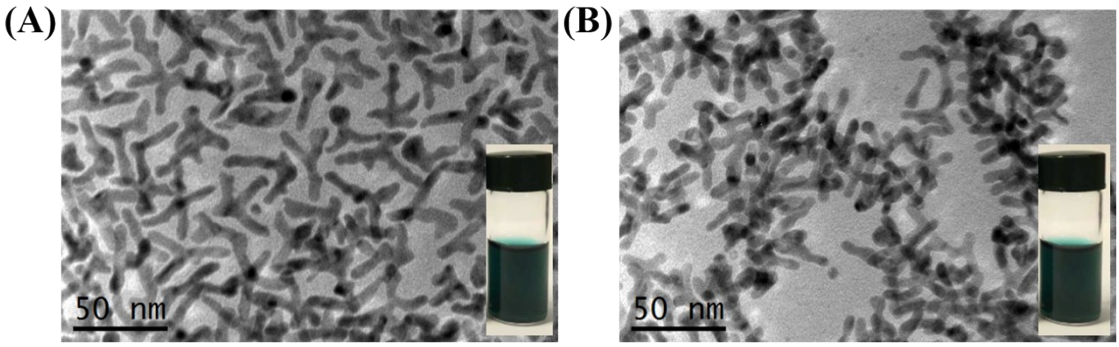

Figure S22. TEM images and photographs (inset) of Au3Cu@PEG-Cy5,FA before (A) and after (B) laser radiation for 40 min.

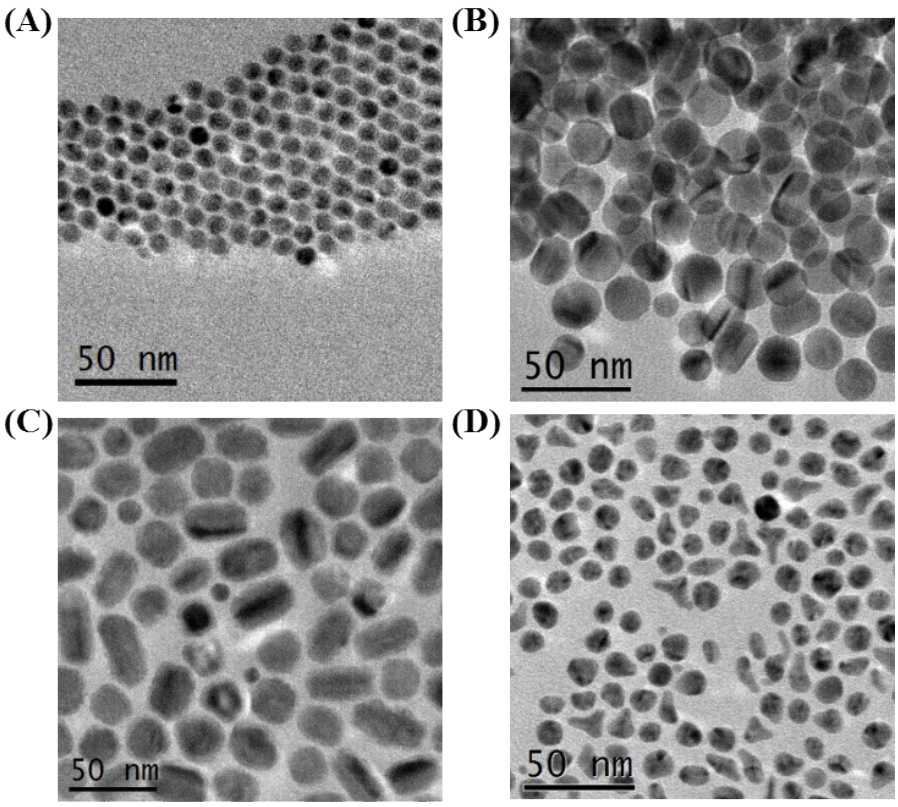

Figure S23. TEM image of (A) Au NPs, (B) $AuCu_3$ NPs, (C) $AuCu_3$ NRs and (D) Deformed Au_3Cu NPs.

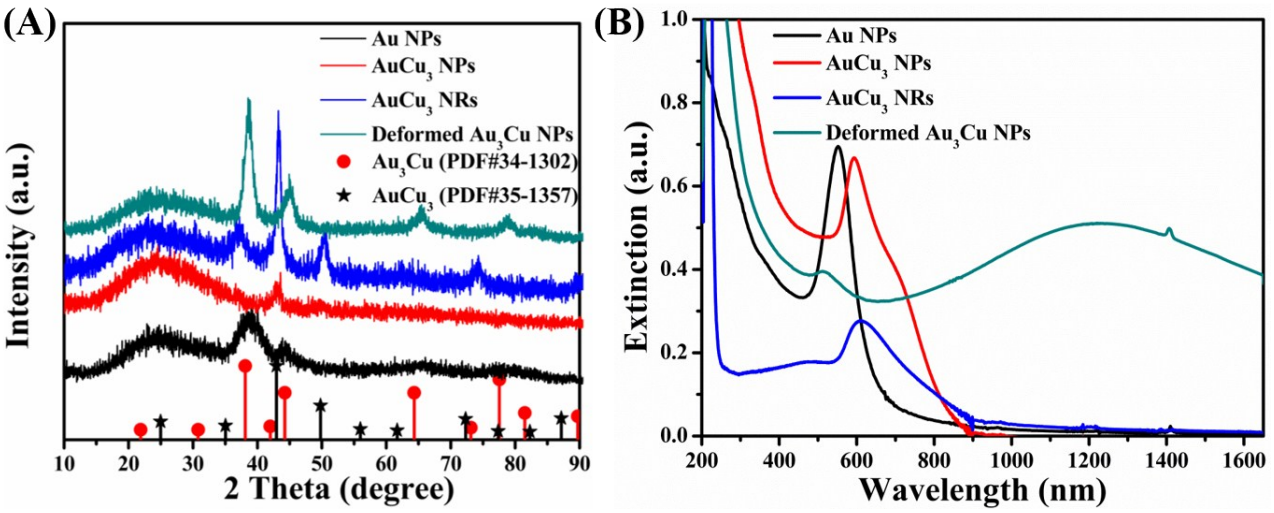

Figure S24. (A) XRD patterns of Au NPs (black line), $AuCu_3$ NPs (red line), $AuCu_3$ NRs (blue line) and Deformed Au_3Cu NPs (green line); (B) UV-Vis-NIR extinction spectra of Au NPs (black line), $AuCu_3$ NPs (red line), $AuCu_3$ NRs (blue line) and Deformed Au_3Cu NPs (green line).

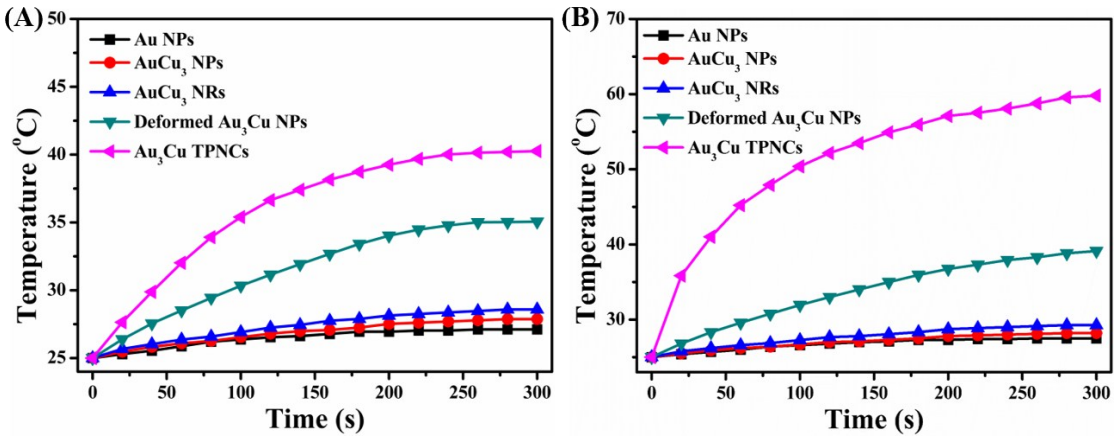

Figure S25. (A) Photothermal heating curves of aqueous suspensions of Au NPs (black line), $AuCu_3$ NPs (red line), $AuCu_3$ NRs (blue line), Deformed Au_3Cu NPs (green line) and Au_3Cu TPNPs (purple line) under irradiation of an 808 nm (NIR-I) and 808 nm (NIR-II) laser at a power density of 1.0 W cm^{-2} for 5 min respectively. (B) Photothermal heating curves of aqueous suspensions of Au NPs (black line), $AuCu_3$ NPs (red line), $AuCu_3$ NRs (blue line), Deformed Au_3Cu NPs (green line) and Au_3Cu TPNPs (purple line) under irradiation of an 1064 nm (NIR-I) and 1064 nm (NIR-II) laser at a power density of 0.8 W cm^{-2} for 5 min respectively.

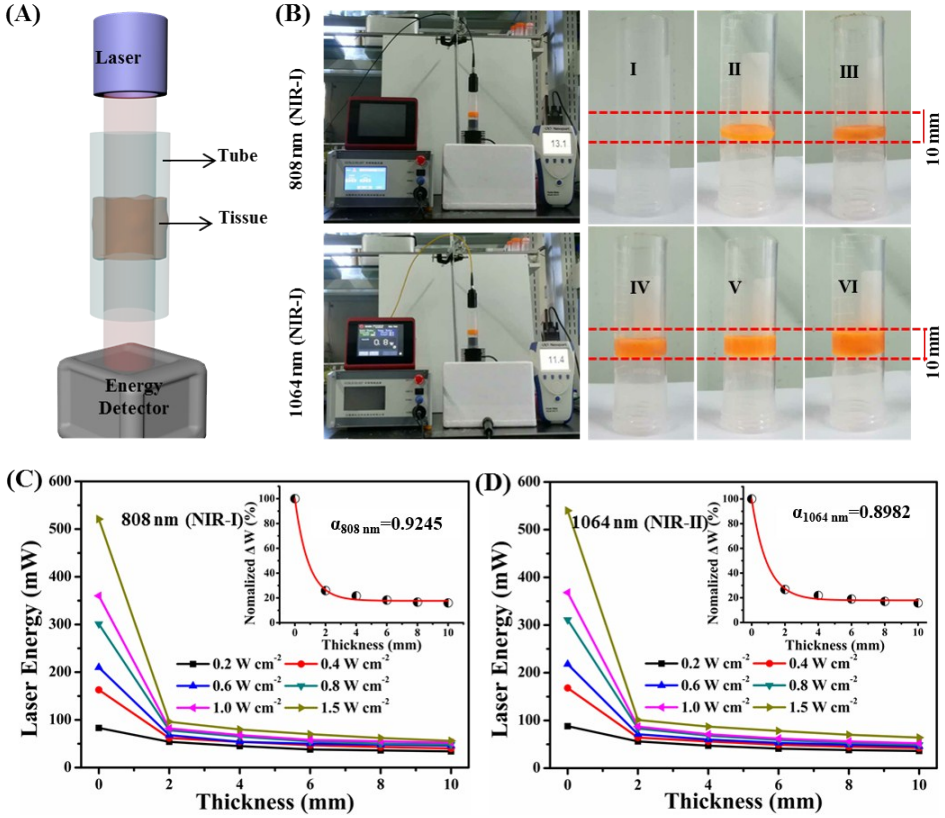

Figure S26. (A) Schematic diagram and (B) Equipment for detecting tissue-penetration capability of NIR laser with different thicknesses (0, 2, 4, 6, 8, and 10 mm) of chicken breast tissues fixed in transparent pipes at 808 and 1064 nm respectively. (C) Energy intensities of NIR-I laser (808 nm) penetrating through tissues of different thickness intervals. Inset: Normalized penetrated NIR-I energy through tissues of different depths. $\alpha_{808\ nm}$: the attenuation coefficient of 808 nm NIR-I laser. (D) Energy intensities of NIR-II laser (1064 nm) penetrating through tissues of different thicknesses. Inset: Normalized NIR-II energy penetrating through tissues of different depths. $\alpha_{1064\ nm}$: the attenuation coefficient of 1064 nm NIR-II laser.

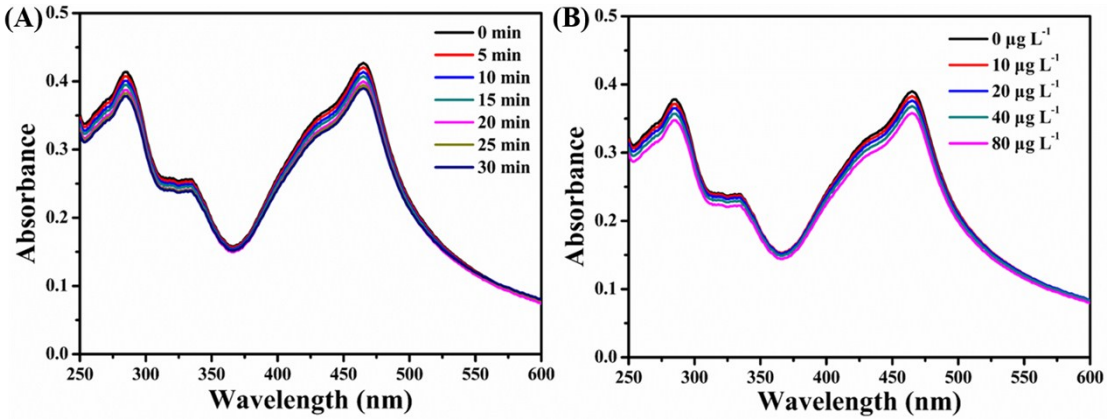

Figure S27. UV-Vis spectrum detection of ROS by DPBF: (A) different incubation time (0, 5, 10, 15, 20, 25 and 30 min) with DPBF after 5 min of 1064 nm laser irradiation with 40 μg mL^{-1} Au_3Cu@PEG and (B) different concentration (0, 10, 20, 40, and 80 μg L^{-1}) of Au_3Cu@PEG in KB cell.

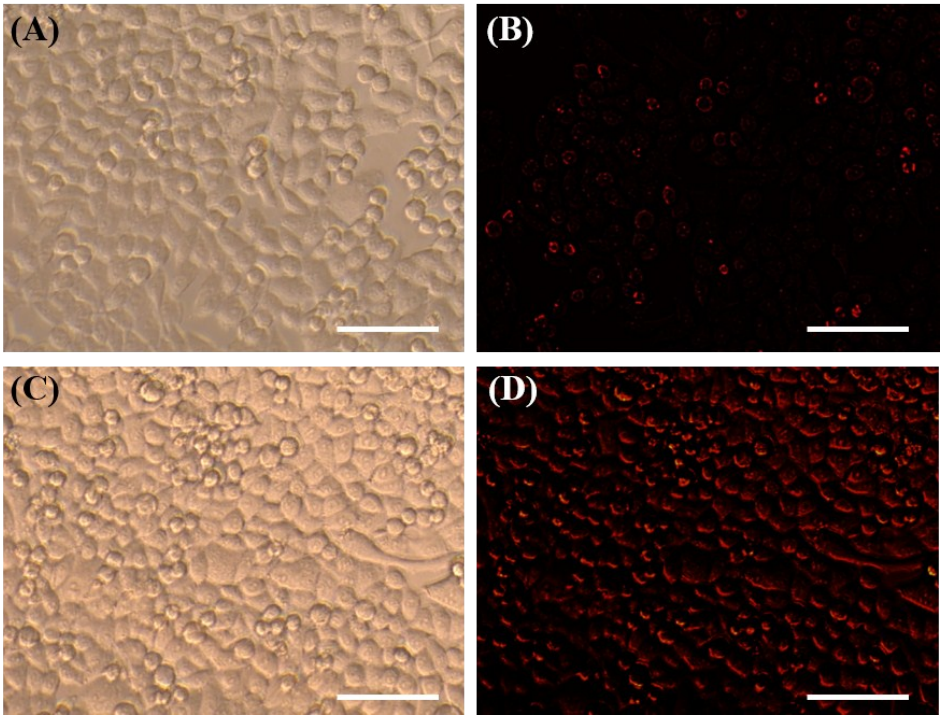

Figure S28. Fluorescence imaging of Au_3Cu@PEG-Cy5 (A), (B) and Au_3Cu@PEG-Cy5,FA (C), (D) in KB cell. (A) and (C) were in bright field, (B) and (D) were in dark field. Scale bars: 100 μm.

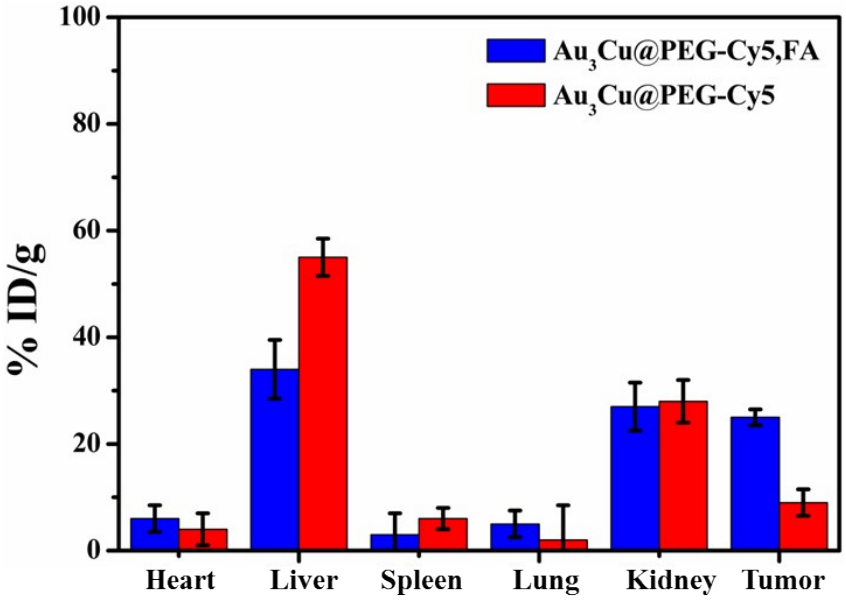

Figure S29. The biodistribution of Au_3Cu@PEG-Cy5 and Au_3Cu-PEG-Cy5,FA with same concentration after i.v. injection for 3 days by ICP-MS.

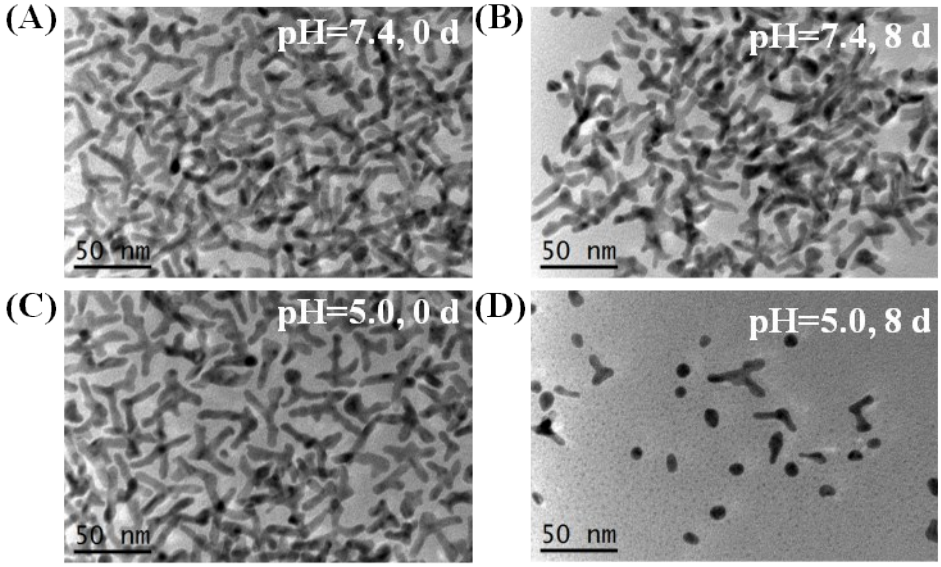

Figure S30. TEM images of Au_3Cu@PEG dispersed in phosphate buffer with different condition: (A) pH=7.4, T=0 d; (B) pH=7.4, T=8 d; (C) pH=5.0, T=0 d; (D) pH=5.0, T=8 d.

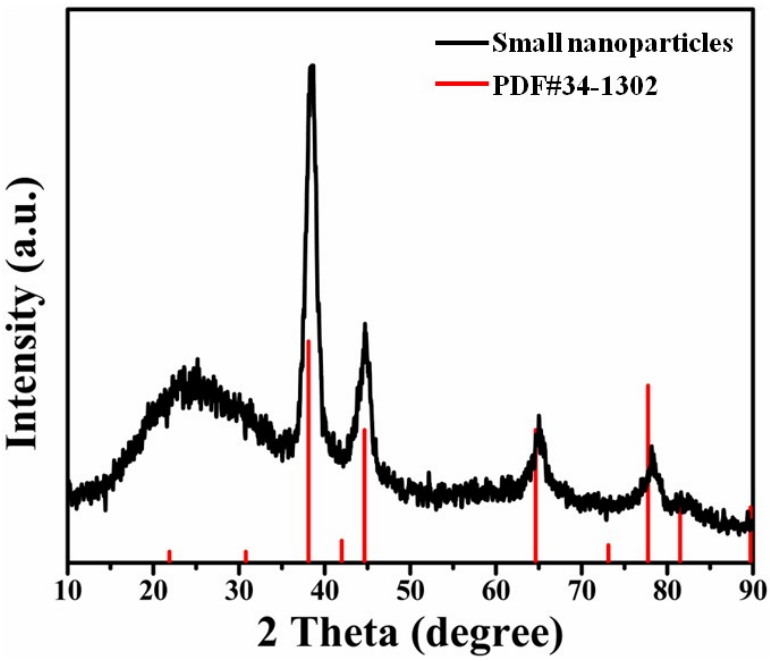

Figure S31. XRD patterns of the collected small nanoparticles under the condition of pH=5.0 after 8 d.

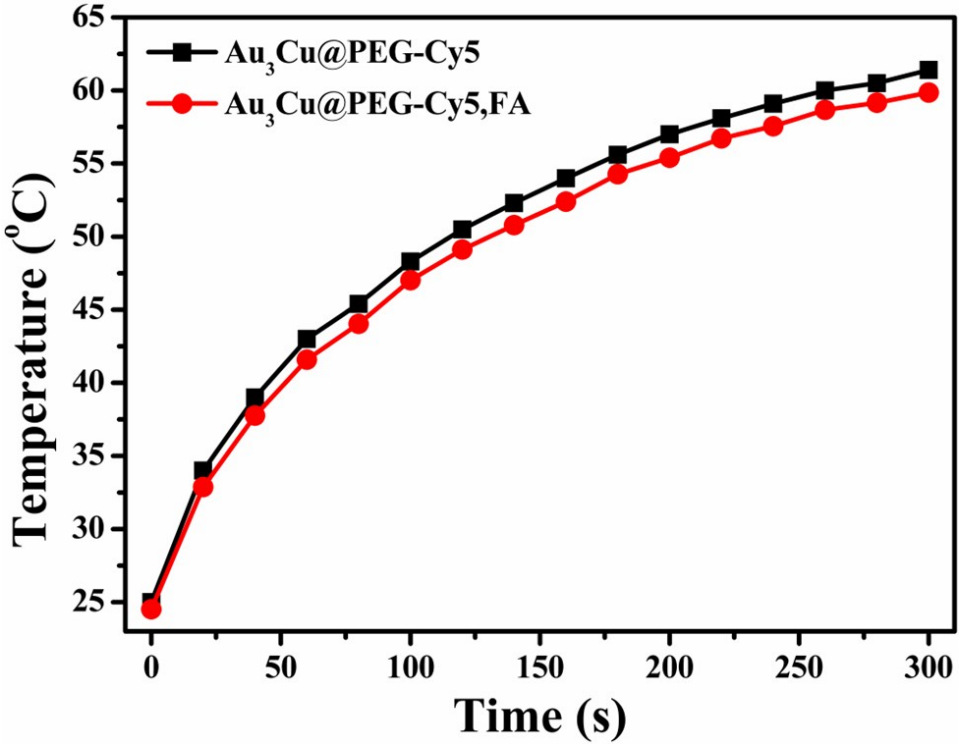

Figure S32. Temperature elevation of Au_3Cu@PEG-Cy5 and Au_3Cu@PEG-Cy5,FA solutions with the same concentration of Au_3Cu (40 μg/mL) under 1064 nm laser irradiation (0.8 W cm^{-2}).

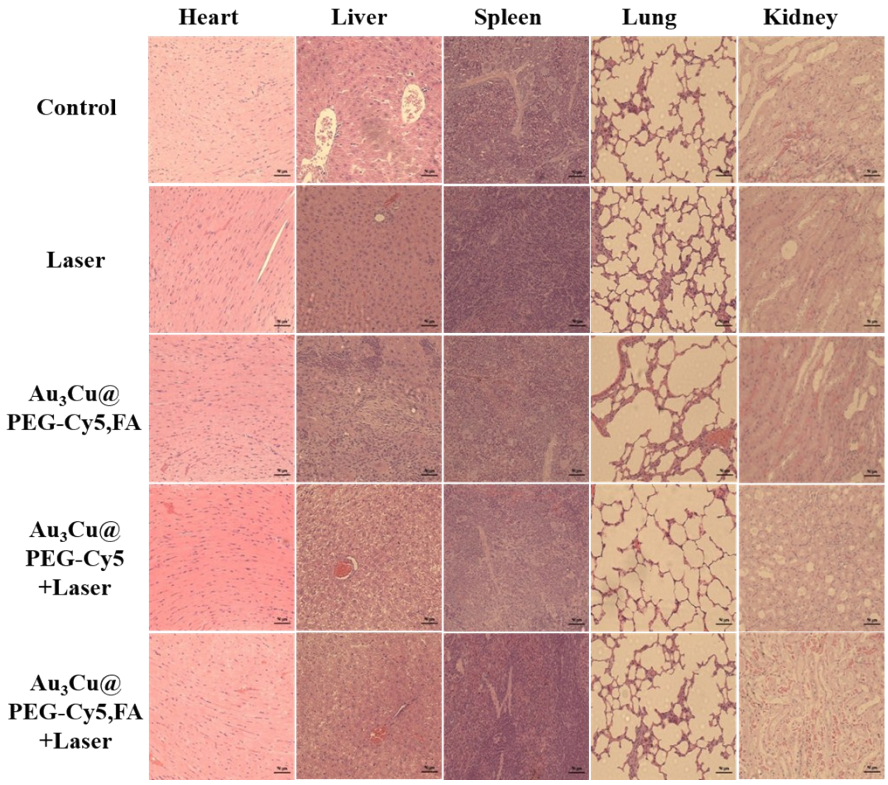

Figure S33. H&E stained images of major organs (heart, liver, spleen, lung, kidney, and intestine) collected from different groups of mice. Bars are 50 μm.

Table S1. ICP-AES results of Au3Cu TPNCs.

Element	Line	Mean（μg/mL）	Atomic percentage (%)	RSD
Au	Au 242.795	1.4439	74.4	0.1893
Cu	Cu 324.754	0.1613	25.6	0.0971

Table S2. Zeta potential of multifuctonal modified Au_3Cu TPNCs.

Sample name	Au_3Cu@PEG	Au_3Cu@PEG-FA	Au_3Cu@PEG-Cy5,FA
Zeta potential (mV)	9.77	1.71	-3.02

Table S3. Zeta potential of Au_3Cu@PEG-Cy5,FA after 14 days in PBS.

Time (day)	0	2	4	6	8	10	12	14
Zeta potential (mV)	-3.02	-3.12	-3.17	-3.13	-3.08	-3.06	-3.09	-3.17

Table S4. The photothermal-conversion efficiency (η) of AuCu-based nanomaterials under the 808 nm laser (1.0 W cm^{-2}).

Sample name	Au NPs	$AuCu_3$ NPs	$AuCu_3$ NRs	Deformed Au_3Cu NCs	Au_3Cu TPNCs
η (%)	5.21	9.54	11.48	22.49	39.45

Table S5. The photothermal-conversion efficiency (η) of AuCu-based nanomaterials under the 1064 nm laser (0.8 W cm^{-2}).

Sample name	Au NPs	$AuCu_3$ NPs	$AuCu_3$ NRs	Deformed Au_3Cu NCs	Au_3Cu TPNCs
η (%)	2.37	4.33	5.34	45.16	75.27

References

1. B. Wang, J. Hai, Q. Wang, T. Li, Z. Yang, *Angew. Chem. Int. Ed.* 2011, **50**, 3063-3066.
2. J. Liu, Z. Li, X. Yang, W. Liu, B. Wang, Y. Zhu, K. Mu, W. Zhu, *Chem. Commun.* 2015, **51**, 13369-13372.
3. L. Zhang, S.-I. Choi, J. Tao, H.-C. Peng, S. Xie, Y. Zhu, Z. Xie, Y. Xia, *Adv. Funct. Mater.* 2014, **24**, 7520-7529.
4. D. Keith Roper, W. Ahn, M. Hoepfner, *J. Phys. Chem. C* 2007, **111**, 3636-3641.
5. Q. Tian, F. Jiang, R. Zou, Q. Liu, Z. Chen, M. Zhu, S. Yang, J. Wang, J. Wang, J. Hu, *ACS Nano* 2011, **5**, 9761-9771.
6. Y. Ju, H. Zhang, J. Yu, S. Tong, N. Tian, Z. Wang, X. Wang, X. Su, X. Chu, J. Lin, Y. Ding, G. Li, F. Sheng, Y. Hou, *ACS Nano* 2017, **11**, 9239−9248.
7. M. Ji, M. Xu, W. Zhang, Z. Yang, L. Huang, J. Liu, Y. Zhang, L. Gu, Y. Yu, W. Hao, P. An, L. Zheng, H. Zhu, J. Zhang, *Adv. Mater*. 2016, **28**, 3094-3101.